

TECHNICAL REPORT BRL-TR-3225

BRL

THE EFFECT OF SABOT WHEELBASE AND
POSITION ON THE LAUNCH DYNAMICS OF
FIN-STABILIZED KINETIC ENERGY AMMUNITION

PETER PLOSTINS
JONATHAN A. BORNSTEIN
ILMARS CELMINS

APRIL 1991

APPROVED FOR PUBLIC RELEASE; DISTRIBUTION IS UNLIMITED.

U.S. ARMY LABORATORY COMMAND

BALLISTIC RESEARCH LABORATORY
ABERDEEN PROVING GROUND, MARYLAND

UNCLASSIFIED

REPORT DOCUMENTATION PAGE			Form Approved OMB No. 0704-0188	
<small>Public reporting burden for this collection of information is estimated to average 1 hour per response, including the time for reviewing instructions, searching existing data sources, gathering and maintaining the data needed, and completing and reviewing the collection of information. Send comments regarding this burden estimate or any other aspect of this collection of information, including suggestions for reducing this burden, to: Washington Headquarters Services, Directorate for Information Operations and Reports, 1215 Jefferson Davis Highway, Suite 1204, Arlington, VA 22202-4302, and to the Office of Management and Budget, Paperwork Reduction Project (0704-0188), Washington, DC 20503.</small>				
1. AGENCY USE ONLY (Leave blank)	2. REPORT DATE April 1991	3. REPORT TYPE AND DATES COVERED Final 1 Jan 90 - 31 Dec 90		
4. TITLE AND SUBTITLE The Effect of Sabot Wheelbase and Position on the Launch Dynamics of Fin-Stabilized Kinetic Energy Ammunition		5. FUNDING NUMBERS 1L162618AH80		
6. AUTHOR(S) Peter Plostins Jonathan A. Bornstein Ilmars Celmins				
7. PERFORMING ORGANIZATION NAME(S) AND ADDRESS(ES) US Army Ballistic Research Laboratory ATTN: SLCBR-LF Aberdeen Proving Ground, MD 21005-5066		8. PERFORMING ORGANIZATION REPORT NUMBER		
9. SPONSORING / MONITORING AGENCY NAME(S) AND ADDRESS(ES) US Army Ballistic Research Laboratory ATTN: SLCBR-DD-T Aberdeen Proving Ground, MD 21005-5066		10. SPONSORING / MONITORING AGENCY REPORT NUMBER BRL-TR-3225		
11. SUPPLEMENTARY NOTES				
12a. DISTRIBUTION / AVAILABILITY STATEMENT Approved for public release; distribution is unlimited.		12b. DISTRIBUTION CODE		
13. ABSTRACT (Maximum 200 words) <p>A test program was performed to determine the effects of changes in sabot wheelbase and position on the launch dynamics of fin-stabilized kinetic energy penetrators. The launch sequence was measured; the measurements covered the gun dynamics, transitional ballistics and free-flight aeroballistics of the projectile trajectory. All of the projectile jump components were measured independently, summed and the result compared with the projectile impact on the target. The dispersion of each of the components was computed and compared to the target impact dispersion. The dispersion computed using the dispersion model compared well with the target impact dispersion. Both low and high dispersion was observed for the different configurations. Low dispersion was the result of strong biases or low component magnitudes. Each configuration responded differently to the inbore launch sequence; therefore, the key to understanding the origins of the dispersion phenomenon lies in understanding the inbore dynamic response of sabot/penetrator designs.</p>				
14. SUBJECT TERMS kinetic energy projectiles; sabots; KE ammunition dispersion; in-bore balloting; KE ammunition jump; sabot design; sabot discard			15. NUMBER OF PAGES 42	
			16. PRICE CODE	
17. SECURITY CLASSIFICATION OF REPORT UNCLASSIFIED	18. SECURITY CLASSIFICATION OF THIS PAGE UNCLASSIFIED	19. SECURITY CLASSIFICATION OF ABSTRACT UNCLASSIFIED	20. LIMITATION OF ABSTRACT Same as Report	

UNCLASSIFIED

INTENTIONALLY LEFT BLANK.

ACKNOWLEDGMENTS

The authors wish to express their appreciation to Mr. Donald McClellan, Mr. William Thompson and Mr. John Carnahan for their efforts during the experimental testing phase of this program. Thanks are also extended to Ms. Emily Hsi for her help in preparing the figures for the report. Special thanks are extended to Mr. Miguel Andriolo for giving some statistical significance to this engineering study.

INTENTIONALLY LEFT BLANK.

TABLE OF CONTENTS

	<u>Page</u>
Acknowledgments	iii
List of Figures	vii
List of Tables	ix
I. Introduction	1
II. Test Instrumentation and Procedures	2
III. Closure and Dispersion Model	3
IV. Analysis of the Data	4
V. Discussion of the Results	5
VI. Conclusions	8
References	35
Distribution List	37

INTENTIONALLY LEFT BLANK.

LIST OF FIGURES

<u>Figure</u>	<u>Page</u>
1a Photograph of the Long, Baseline and Short Wheelbase Configurations	9
1b Photograph of the Sabot-Rear, Baseline and Sabot-Forward Configurations	10
2 Schematic of the Test Set-Up	11
3 Closure Model	12
4 Dispersion Model	13
5 Horizontal and Vertical Pointing Angle	14
6 Horizontal CG Trajectory of the Projectile	15
7 Vertical CG Trajectory of the Projectile	16
8a Vertical X-Ray Image of the Long Wheelbase Design: X-Ray Station # 1	17
8b Vertical X-Ray Image of the Long Wheelbase Design: X-Ray Station # 2	18
8c Vertical X-Ray Image of the Long Wheelbase Design: X-Ray Station # 3	19
8d Vertical X-Ray Image of the Long Wheelbase Design: X-Ray Station # 4	20
8e Vertical X-Ray Image of the Long Wheelbase Design: X-Ray Station # 5	21
8f Vertical X-Ray Image of the Long Wheelbase Design: X-Ray Station # 6	22
9 Horizontal Yawing Motion	23
10 Vertical Yawing Motion	24
11 Jump Closure	25
12 Muzzle Pointing Angle Summary	26
13 Muzzle Crossing Velocity Summary	27
14 Projectile Center of Gravity Jump Summary	28

LIST OF FIGURES
(continued)

<u>Figure</u>	<u>Page</u>
15 Projectile Aerodynamic Jump Summary	29

I. INTRODUCTION

The inbore dynamic path traversed by the elastic sabot/penetrator assembly is the forcing function that defines the dynamic state of the sabot/penetrator at shot exit. The dynamic state of the sabot/penetrator assembly determines the initial conditions of the transitional ballistic phase and contains the asymmetries imparted to the assembly by the inbore balloting. During the transitional ballistic phase (i.e., the sabot discard) the dynamic state and asymmetries are affected by the mechanical and aerodynamic disturbances caused by the sabot separation. All of the launch disturbances combine to determine the dynamic state of the penetrator as it enters free-flight.

A test was conducted in the Aerodynamics Range Facility of the U.S. Army Ballistic Research Laboratory to assess the effects of different sabot configurations and positions on the launch of long rod penetrators. This test was the second of a series of studies designed to look at the entire launch process of fin-stabilized kinetic energy ammunition. The results of the first test, that examined the effects of changing the sabot front borerider stiffness, were reported in Reference (1). Three conclusions were reached in that study:

- 1.) The linear and angular dynamic states of the projectile at shot exit are not dominated by the motion of the gun muzzle but primarily dependent on the motion of the projectile relative to the bore centerline (i.e. the inbore balloting motion).
- 2.) The front borerider stiffness clearly affects the inbore response of the projectile.
- 3.) The dispersion of the ammunition is a result of a complex interaction determined by the dynamic state of the projectile at muzzle exit.

The third conclusion warrants further discussion. It was found in Reference (1) that a beneficial cross correlation between the projectile center-of-gravity jump at the muzzle (the center-of-gravity jump is defined as the initial deviation of the projectile center-of- gravity at muzzle exit) and the projectile aerodynamic jump was the reason for the lower dispersion. The dispersion of the individual components of jump had not significantly changed for the three borerider stiffnesses tested. Unfortunately, the Reference (1) study, though able to explain the dispersion phenomenon, was unable to suggest sabot design criteria.

The present report presents the results of a series of tests designed to extend the work of Reference (1). Four sabot configurations were tested: 1) a long wheelbase sabot, where the term wheelbase refers to the separation between the front and rear boreriding surfaces, 2) a short wheelbase sabot, 3) a sabot positioned further forward on the penetrator and 4) a sabot positioned further aft on the penetrator. All of the sabot configurations tested were used to launch

an identical fin-stabilized long rod penetrator from a 25mm Mann Barrel. Five projectiles of each configuration were tested. The configurations are shown in Figure (1a) and (1b). In Figure (1a) are the long wheelbase, the baseline case from Reference (1) and the short wheelbase and in Figure (1b) are the sabot-rear, baseline and sabot-forward configurations.

II. TEST INSTRUMENTATION AND PROCEDURES

A schematic of the test set-up is given in Figure (2); it is almost identical to the set-up used in Reference (1). The main difference is that in Reference (1) the gun was fired by pulling a lanyard and for this test the gun was fitted with an electric solenoid to strike the firing pin. It was found that the consistency of the gun dynamics prior to shot exit were improved by changing to the electric firing circuit. A different borescope was also used because the borescope used in Reference (1) was so heavy it changed the pointing angle of the gun. The clearances in the recoil system were removed and consequently the lighter borescope did not affect the gun pointing angle.

The sub-projectile or penetrator launched by the four sabot configurations had a length to diameter ratio (L/D) of 18.5 and was identical in each design except for the buttress groove locations. These had to be shifted to position the sabot forward or aft. The changes in the sabot configurations are relative to the baseline configuration presented in Reference (1). The sabot wheelbase of the baseline configuration is 5.06 penetrator diameters (calibers). The long wheelbase design is 6.05 calibers and the short design is 4.06 calibers. The aft sabot is positioned one caliber aft of the baseline sabot position and in the final design the sabot is positioned one caliber forward of the baseline position. Even with these design variations, the maximum deviation of the sabot/penetrator assembly center-of-gravity from that of the baseline configuration was 4.7%. The maximum deviation of the assembly inertial properties was 7.5% for the transverse moment of inertia. The long wheelbase design had the largest assembly transverse moment of inertia.

The dynamics of the muzzle prior to shot exit were measured by Scientific-Atlanta Model 61 eddy current proximity probes. These were located at the same two positions used in the previous test (i.e. 10.7 cm and 20.8 cm from the muzzle). The mounting of the probes, triggering system, signal processing and data reduction techniques used were briefly discussed in Reference (1) and presented in detail in Reference (2).

The projectiles were launched at a nominal muzzle velocity of 1550 m/s; this is approximately 25 m/s faster than in Reference (1). The dynamics of the projectile during the transitional ballistic phase were recorded by six orthogonal x-ray stations located at 0.032, 0.36, 0.75, 1.25, 1.63 and 2.01 metres downrange from the muzzle. Again the data acquisition and reduction technique was reviewed in Reference (1) and comprehensively discussed in References (3) and (4).

The target impact dispersion was obtained by placing a target in the last aerodynamics range station of the fifth group, at a point 100 metres from the muzzle. The collimated bore-scope was utilized to position the target center on the pre-shot line-of-fire. The coordinates of the target aimpoint and of the muzzle were used to compute the pre-shot line-of-fire.

The Aerodynamics Range Facility, described in Reference (5), was used to record the free-flight trajectory of the penetrator. Reference (6) derives the theory and discusses the data reduction techniques used to obtain the aerodynamic coefficients of the penetrator. These coefficients are required to compute the aerodynamic jump, which is also one of the components of the dispersion.

III. CLOSURE AND DISPERSION MODEL

A review of the closure and dispersion model presented in Reference (1) is necessary because it is the basis for analyzing the results. The closure model defines a series of jump components, along with the gravity drop, whose vector sum equals the location of the fall of shot relative to the pre-shot line-of-fire. A jump vector is a vector whose magnitude is the angle, in milliradians, of the deviation between the projectile trajectory and the line-of-fire. The orientation of the jump vector in a X-Y coordinate system is the arctangent of the ratio of the vector's vertical to horizontal component. The closure model for fin-stabilized sabot-launched kinetic energy penetrators consists of six vectors. These are given in Figure (3). The first is the muzzle-pointing angle (MP) at shot exit; the second is the angle defined by the ratio of transverse velocity of the muzzle to the projectile launch velocity or the "muzzle-crossing velocity jump (CV);" the third is the angular deviation of the projectile center-of-gravity (CG) from the instantaneous bore centerline at shot exit; the fourth is the deviation of the center-of-gravity (SD) due to sabot discard disturbances; the fifth is the aerodynamic jump (AJ) and the sixth is the trajectory drop due to the force of gravity (GD). The last component is not considered a jump component but is included to achieve closure. It can, however, affect the dispersion if a large variation in muzzle velocity is present. The first five components have been found to be the primary jump components required to define the fall of shot for a sabot-launched kinetic energy penetrator and are discussed at length in Reference (1).

The dispersion model is a simple extension of the closure model and is portrayed in Figure (4). The dispersion of the ammunition is scattered about a center of impact on the target. Each impact is the sum of a separate series of jump components. Each individual group of jump components has its own dispersion. Mathematically the target impact dispersion, σ , can be related to the dispersion of the jump components by the relation

$$\sigma^2 = \sum_{i=1}^n \sum_{j=1}^n \sigma_{ij} \quad (1)$$

where

$$\sigma_{ii} = \sigma_i^2 \quad \text{and} \quad \sigma_{ij} = \sigma_{ji}$$

For $i \neq j$, the σ_{ij} terms result from cross correlations between jump components. Statistically cross correlations can exist between all of the jump components but this is a phenomenon that occurs sequentially in time, so a proper physical interpretation of the cross correlation term is necessary. It is not physically possible for the aerodynamic jump component to affect a change in the center-of-gravity component; it is only possible for the center-of-gravity component to affect the aerodynamic jump component, because the latter occurs at a later time. The preceding model is the basis for the analysis of the test data in the next section.

IV. ANALYSIS OF THE DATA

The dispersion analysis requires that a jump history of each projectile fired be computed. The muzzle-pointing angle and crossing velocity jump components were computed from the proximity probe data. Figure (5) presents the horizontal and vertical pointing angle history for the launch of a long wheelbase sabot/penetrator assembly, round number 19418. Shot exit occurs at approximately $t = -0.06$ milliseconds. The inbore time for the projectile is two milliseconds. Figures (6) and (7) give horizontal and vertical x-ray and Aerodynamics Range center-of-gravity trajectory data for the same round. The reference line for the jump is the line-of-fire defined in the figures by the solid line connecting the "X" symbols. The square symbols represent the x-ray data, the circles represent the Aerodynamics Range data and the solid curve represents the Aerodynamics Range data reduction fit of the swerve data. Both the free-flight data and the x-ray data fall on the swerve curve. The dashed line is the tangent to the swerve curve at the muzzle and the angle between it and the line-of-fire is the center-of-gravity jump component. Figures (8a) through (8f) are vertical x-ray images of the sabot discard of the long wheelbase sabots from the penetrator of round number 19418. Although the sabots have mechanically disengaged from the penetrator, they are still in aerodynamic contact. Free flight is achieved between the last x-ray station and the first Aerodynamics Range station. The angular motion of the penetrator is presented in Figures (9) and (10). The Aerodynamics Range data fit of the yawing motion also fits both the x-ray and free-flight data. Therefore, as observed in Reference (1), the coincidence of the x-ray data with the free-flight yaw fit leads to the conclusion that there were no sabot discard disturbances and the sabot discard jump component and dispersion can be dropped from the subsequent analysis.

The five component closure is plotted in Figure (11). The sabot discard jump was zero and does not appear in the plot. Note that the jump due to the gun dynamics is too small to identify. The closure plot is constructed by extrapolating the gun dynamics jump components forward from the origin and then extrapolating the gravity drop and aerodynamic jump components backwards from the target impact. Closure is achieved by subtracting these components

from the total jump and computing the missing center-of-gravity jump component. Closure is independently confirmed by plotting the computed center-of-gravity jump obtained on the horizontal and vertical swerve data in Figures (6) and (7). The center-of-gravity jump should be tangent to the swerve curve at the muzzle. The dashed line marked "CG JUMP" in the figures is, as expected, tangent to the swerve curve. The jump closure for each projectile fired was computed as described above.

V. DISCUSSION OF THE RESULTS

Only five rounds of each configuration were tested. Complete data was obtained on all rounds except one of the sabot-rear configuration. Gun dynamics data was lost on this shot. To complete the data reduction procedure for this projectile, the mean gun dynamics obtained from the other four rounds of that configuration was used. This allowed the jump closure to be approximated without changing the dispersion results significantly. Table (1) presents the target impact dispersion in milliradians of the four configurations and the mean impact locations. Each configuration has a different mean impact location and dispersion. The long wheelbase configuration has the lowest dispersion. All of the other configurations have high dispersion except for the vertical component of the sabot forward configuration.

The launch muzzle velocity had very low variability for all the projectiles fired so the dispersion in the gravity drop has been ignored. Figures (12), (13), (14) and (15) are summary plots of the four jump components. The magnitude and direction of each component is plotted in the figures. Figure (12) presents the muzzle-pointing angle jump. The data is of the same magnitude as that reported in Reference (1) but opposite in direction. The change is probably due to the alterations to the firing and recoil system discussed earlier. The muzzle-crossing velocity, Figure (13), is of the same magnitude and direction as that reported in Reference (1) but, except for one point, is more consistent. Both quantities are so small in magnitude that their influence on the overall dispersion is very small. An interesting item to note is that the muzzle-crossing velocity of the long wheelbase design is much smaller relative to the other configurations. Figure (14), a plot of the projectile center-of-gravity jump component, is revealing because in Reference (1) the component is also biased to the upper half quadrant and the same result is observed again. It appears this Mann barrel has an interior ballistic dynamic path that launches sabot kinetic energy penetrators with a center-of-gravity motion biased up for seven different sabot configurations, the three reported in Reference (1) and the four reported in this paper. All of the center-of-gravity jump components appear randomly distributed within the bias except for the long sabot wheelbase component. This component has a very strong vertical bias and is almost constant in magnitude relative to the other three components. Figure (15) plots the aerodynamic jump components of the four configurations; it appears randomly distributed in magnitude and direction. As observed in Reference (1), the gun motion is an order of magnitude smaller than either the center-of-gravity jump or the aerodynamic jump. The conclusion is again reached that the linear and angular dynamics of the projectile at the muzzle

is a result of the inbore balloting of the projectile and not imposed by the motion of the gun muzzle itself.

Tables (2), (3), (4) and (5) summarize the dispersion of each component for each configuration tested and compare the results with the actual target impact dispersion. The dispersion model used to generate the tables is given by Equation (2):

$$\sigma^2 = \sigma_{MP}^2 + \sigma_{CV}^2 + \sigma_{CG}^2 + \sigma_{AJ}^2 + 2\sigma_{CGAJ} \quad (2)$$

The only cross correlation included in this model is the center-of-gravity/aerodynamic jump term. Since there are no sabot discard disturbances, the two components are physically coupled because they are excited by the same interior ballistic forcing function (i.e. the dynamic and static curvature of the gun tube). The other cross correlations may exist but can be eliminated by the statistical and physical arguments discussed in Reference (1) and later in this section. In all cases, the total dispersion from the components evaluated using Equation (2) is within statistical limits for the measured target impact dispersion. The χ^2 test, see Reference (7), applied to the measured target impact dispersion for an 80% confidence interval yields the following results: for five data points and the smallest dispersion measured ($\sigma=0.23$) the interval is $0.16 < \sigma < 0.45$ and for the largest dispersion measured ($\sigma=0.70$) the interval is $0.50 < \sigma < 1.09$. All of the dispersion data in Tables (2), (3), (4) and (5) fall well within these bounds. Considering the low number of data points in each group, the model appears to adequately describe the physics of the dispersion phenomenon.

The data in Tables (2) through (5) confirm that the gun motion is a small contributor to the dispersion. The primary reason for this is that the magnitude of the gun dynamics is very small. Statistically significant cross correlations were found between the muzzle-pointing angle and the muzzle-crossing velocity as well as between the muzzle-crossing velocity and the center-of-gravity jump. These correlations are physically possible. Clearly, the muzzle-pointing angle and crossing velocity are coupled. There is an exchange of linear momentum between the balloting sabot/penetrator assembly and the gun barrel during the inbore trajectory, therefore, the muzzle-crossing velocity could be coupled to the center-of-gravity motion of the projectile at shot exit. However, the computed covariances for these correlations were so small, they were not essential to the analysis and thus not considered. The covariance for the center-of-gravity/aerodynamic jump component is included in the tables. All of these cross correlations except one were found to be statistically insignificant. This fact is marked in the tables by the asterisk. They were included because they produce the largest covariances, contribute substantially to the sum evaluated by using Equation (2) and are physically possible.

The data for the long wheelbase design in Table (2) has no statistically significant cross correlation terms and has low dispersion. This is quite different from the results of Reference (1), where the stiff front borerider design had low dispersion due to a fortuitous cross correlation. The short wheelbase configuration, Table (3), displays double the dispersion in both the

center-of-gravity and aerodynamic jump components. For the sabot-rear configuration, Table (4), the center-of-gravity jump component dispersion is also high and the dispersion of the horizontal component of the aerodynamic jump is smaller. The final configuration, the forward-sabot, Table (5), has low center-of-gravity component dispersion but enhanced aerodynamic jump component dispersion. In the vertical plane, there is a statistically significant negative cross correlation, reducing the dispersion to the target impact value.

The lower dispersion of the long wheelbase configuration is due to the low dispersion of the center-of-gravity jump component. It is essential to note that this is not because the center-of-gravity jump for that configuration has a small magnitude, see Figure (14), but because it has low variability in magnitude and direction. The low dispersion of the center-of-gravity components of the sabot-forward configuration, Figure (14), stems from the components having a low magnitude despite having a significantly higher variability in direction.

The penetrators fired during this test program were all launched with yaw levels of less than three degrees of first maximum yaw. Launch of kinetic energy penetrators at yaw levels of less than three degrees is generally considered excellent. Yet at least three of the configurations showed large dispersion. Because there are no sabot discard disturbances, the aerodynamic jump is linearly proportional to the angular rate of departure of the projectile at the muzzle or the first maximum yaw. Despite the low yaw launch levels, there was both large and small dispersion exhibited by the aerodynamic jump components. Consider the dispersion of the vertical aerodynamic jump component of the short wheel base configuration and the dispersion of the horizontal aerodynamic jump component of the sabot-rear configuration, the former is large and the latter is small. The lower dispersion of the horizontal aerodynamic jump component of the sabot-rear configuration, see Figure (15), is a result of the low variability in direction of the component. Its bias is within the lower right quadrant. The vertical aerodynamic jump component of the short wheelbase configuration is scattered across three quadrants in Figure (15).

VI. CONCLUSIONS

The research reported in this study is part of a continuing effort to understand the factors affecting the launch dynamics, accuracy and dispersion characteristics of fin-stabilized kinetic energy ammunition. Specific design changes were made to the sabot/penetrator assembly to alter the inbore response and thus study the resultant effects. Regrettably, as found in Reference (1), no simple design criteria can be suggested. The jump and dispersion characteristics of the ammunition can be explained using the dispersion model originally proposed by the authors in Reference (1). It is possible using the techniques described to measure not only the jump components but also the dispersion components of ammunition. Low dispersions were observed for two reasons; one, there was low variability with large magnitude or two, the magnitude of the components were small despite significant variability in direction. The ability to control the dispersion of sabot - launched kinetic energy penetrators lies in the understanding of the inbore dynamic response of the sabot penetrator assembly to the interior ballistic forcing function.

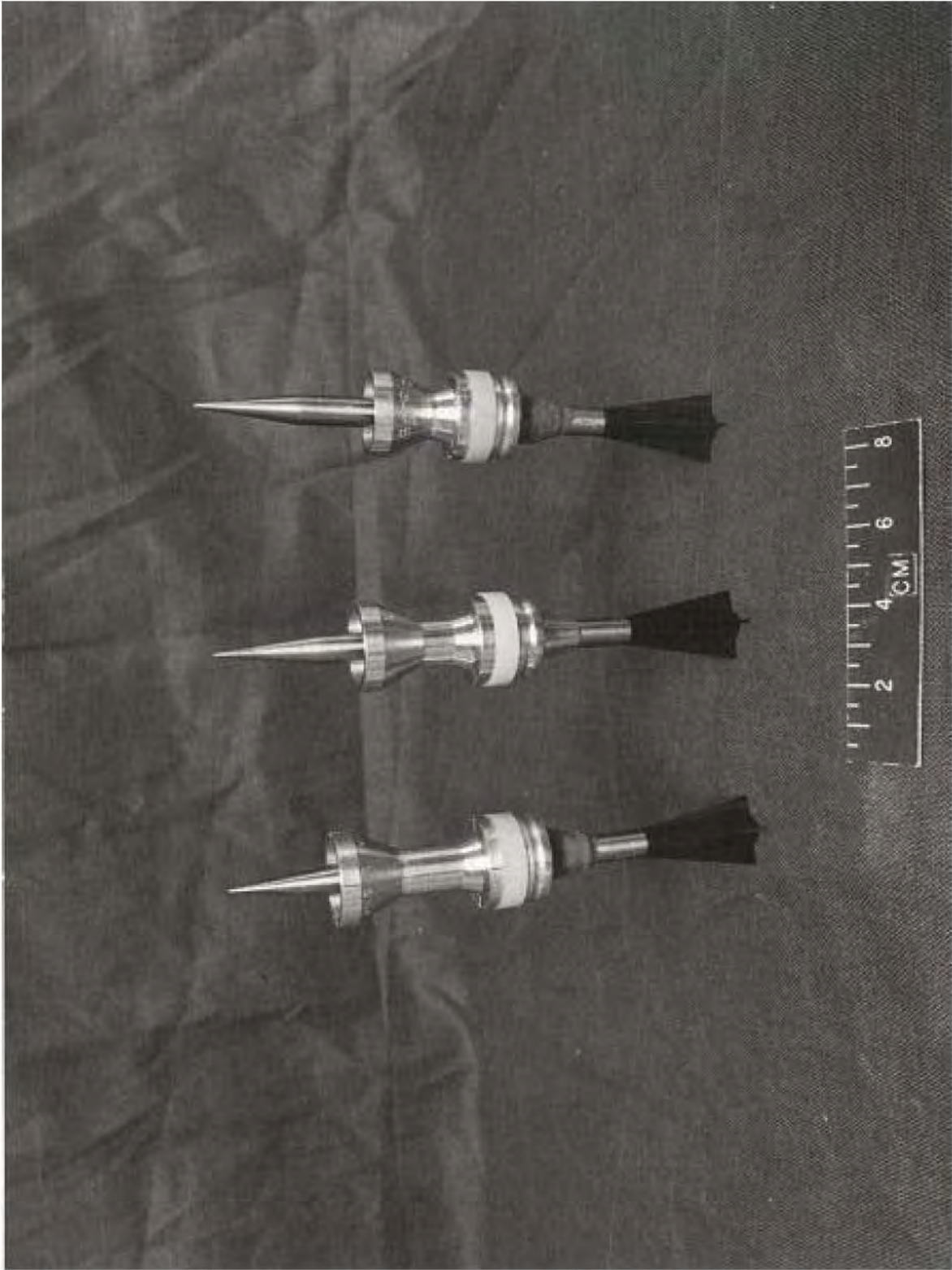


Figure (1a) Photograph of the Long, Baseline and Short Wheelbase Configurations

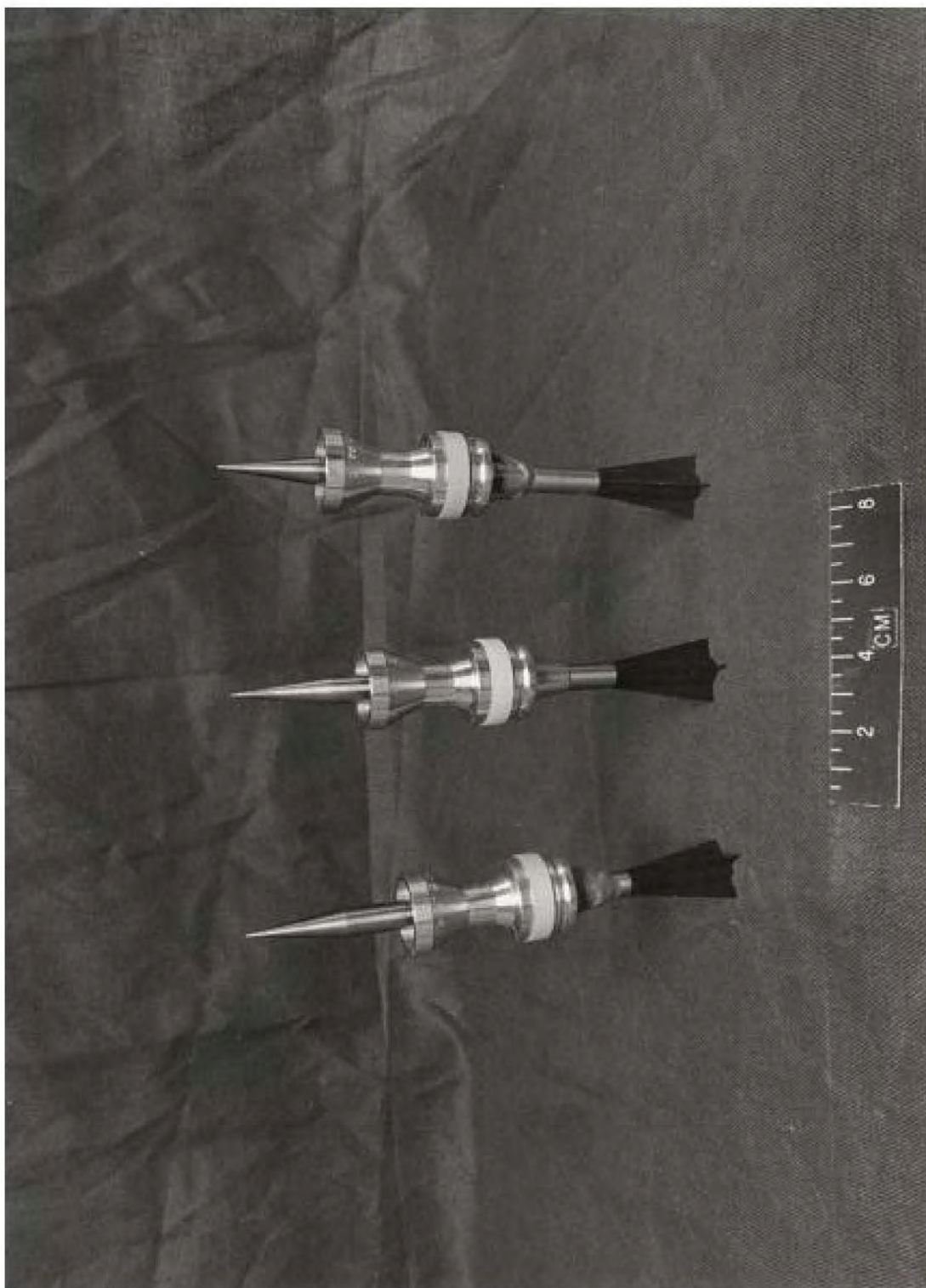


Figure (1b) Photograph of the Sabot-Rear, Baseline and Sabot-Foreward Configurations

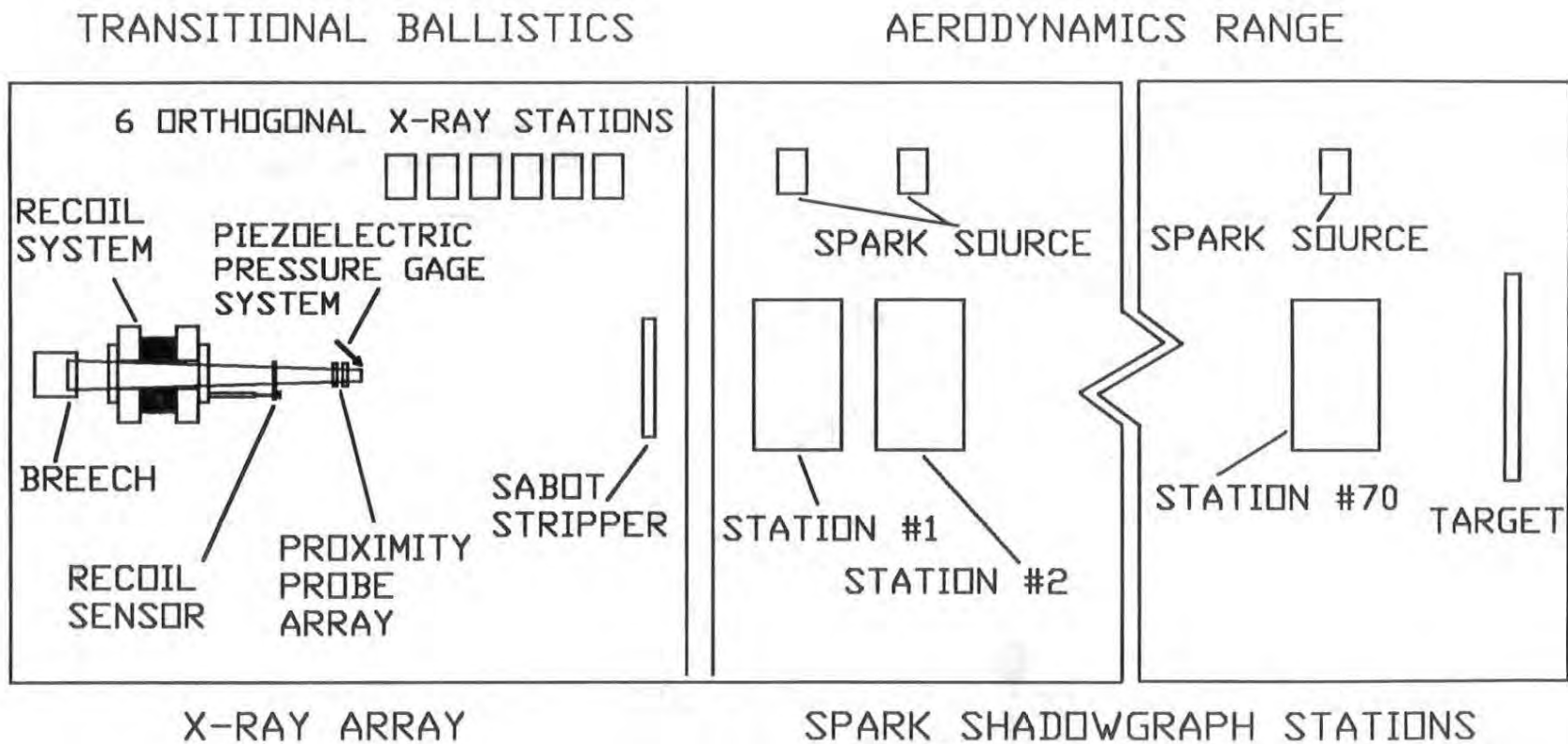


Figure (2) Schematic of the Test Set-Up

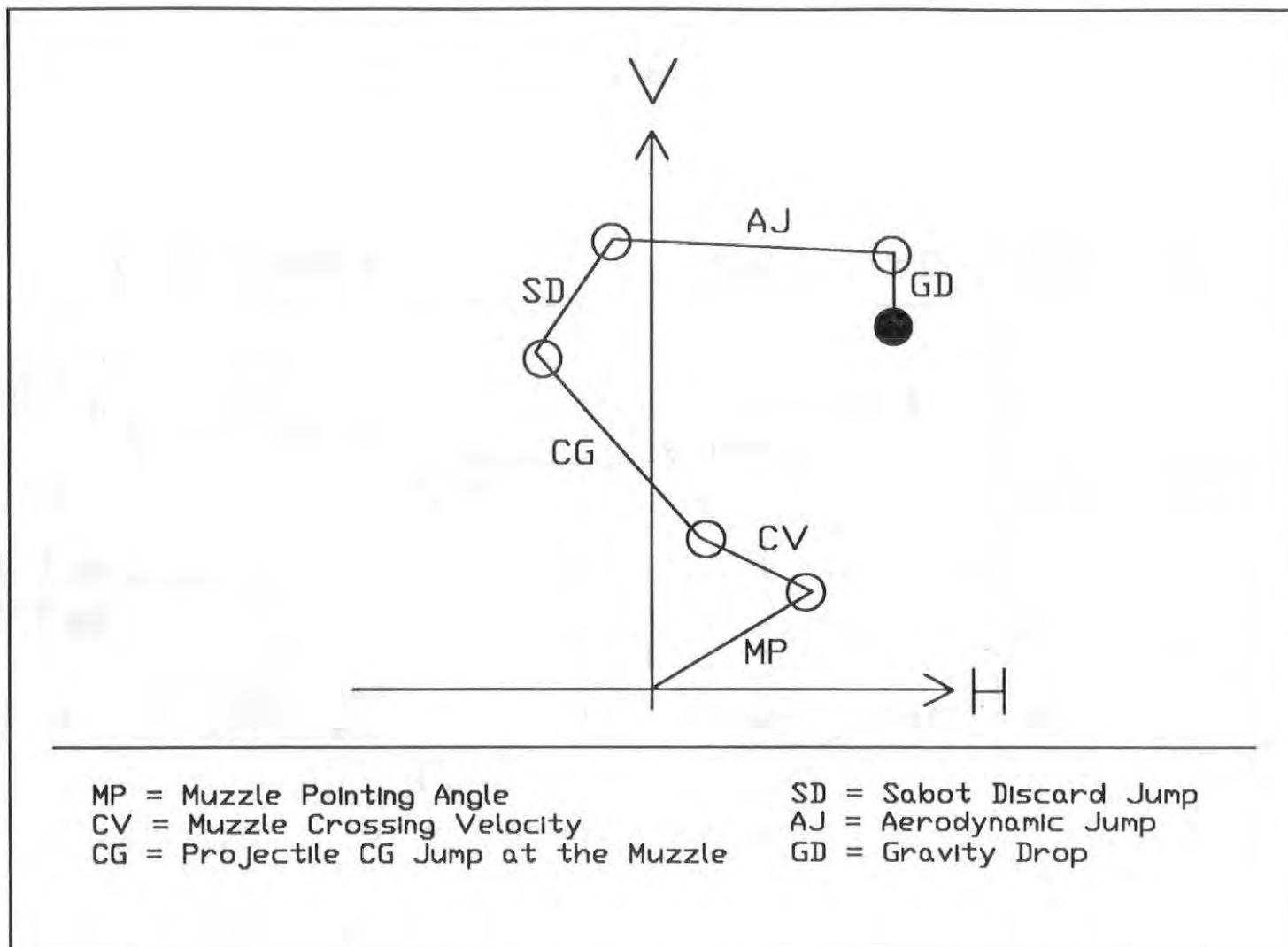


Figure (3) Closure Model

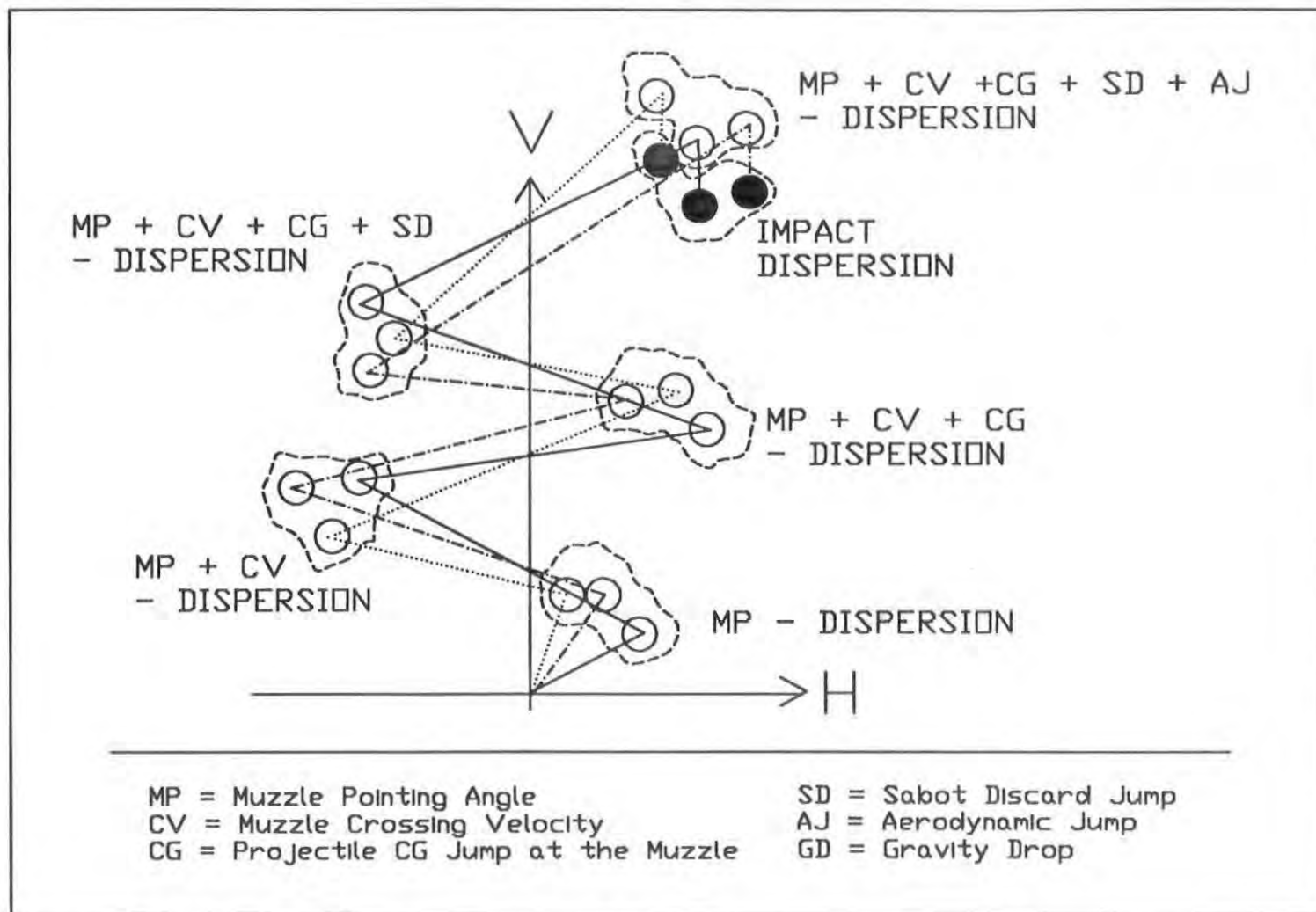


Figure (4) Dispersion Model

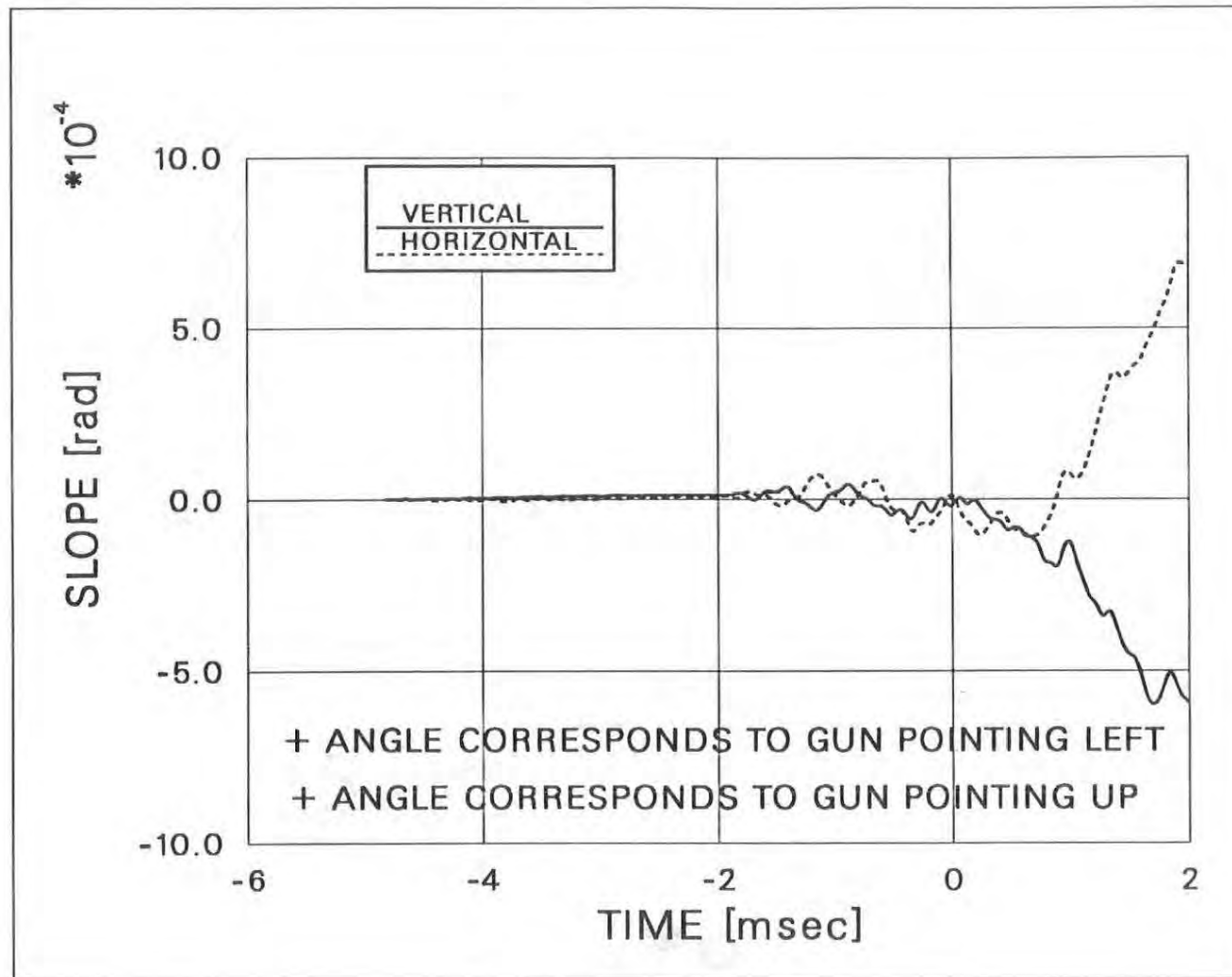


Figure (5) Horizontal and Vertical Pointing Angle

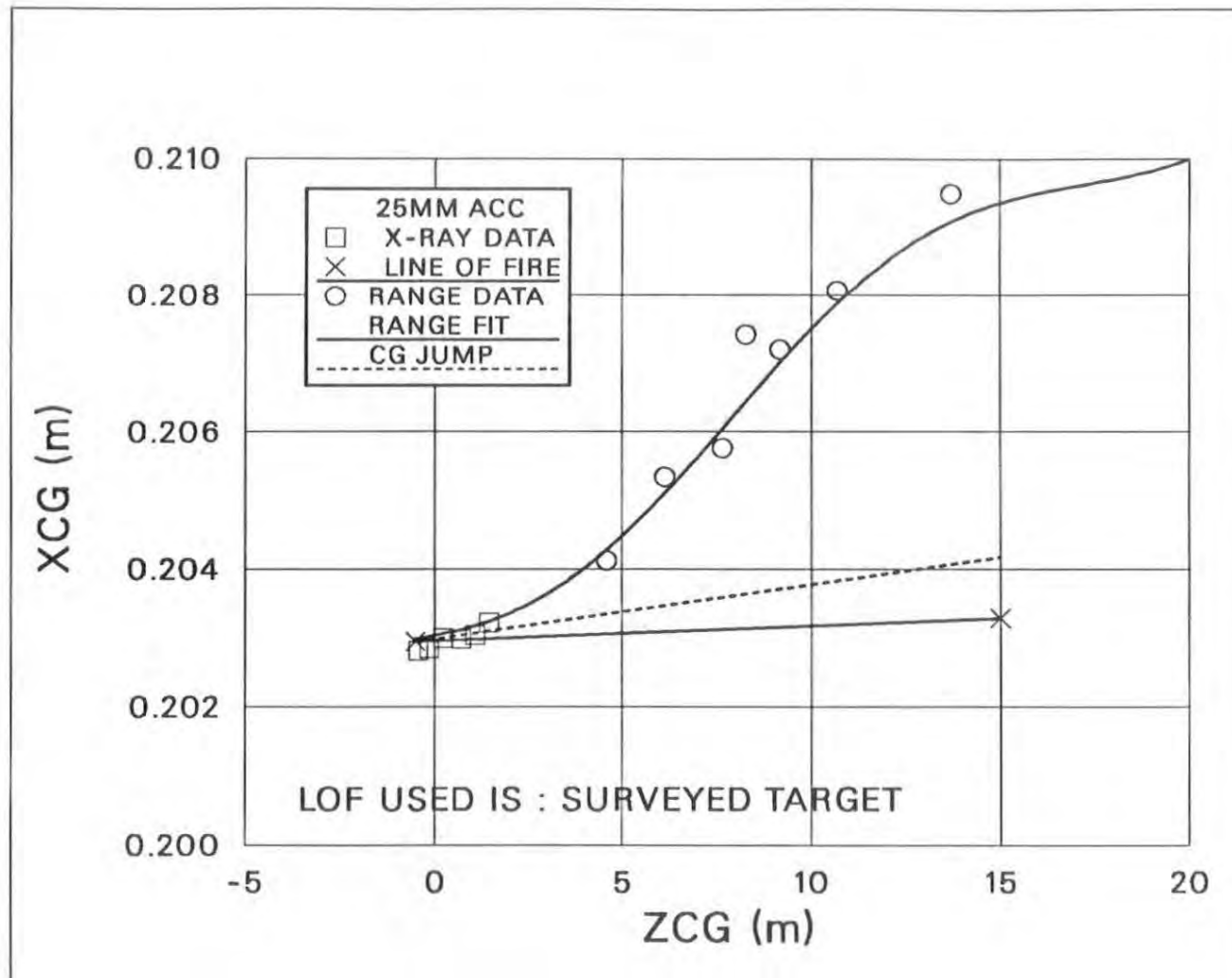


Figure (6) Horizontal CG Trajectory of the Projectile

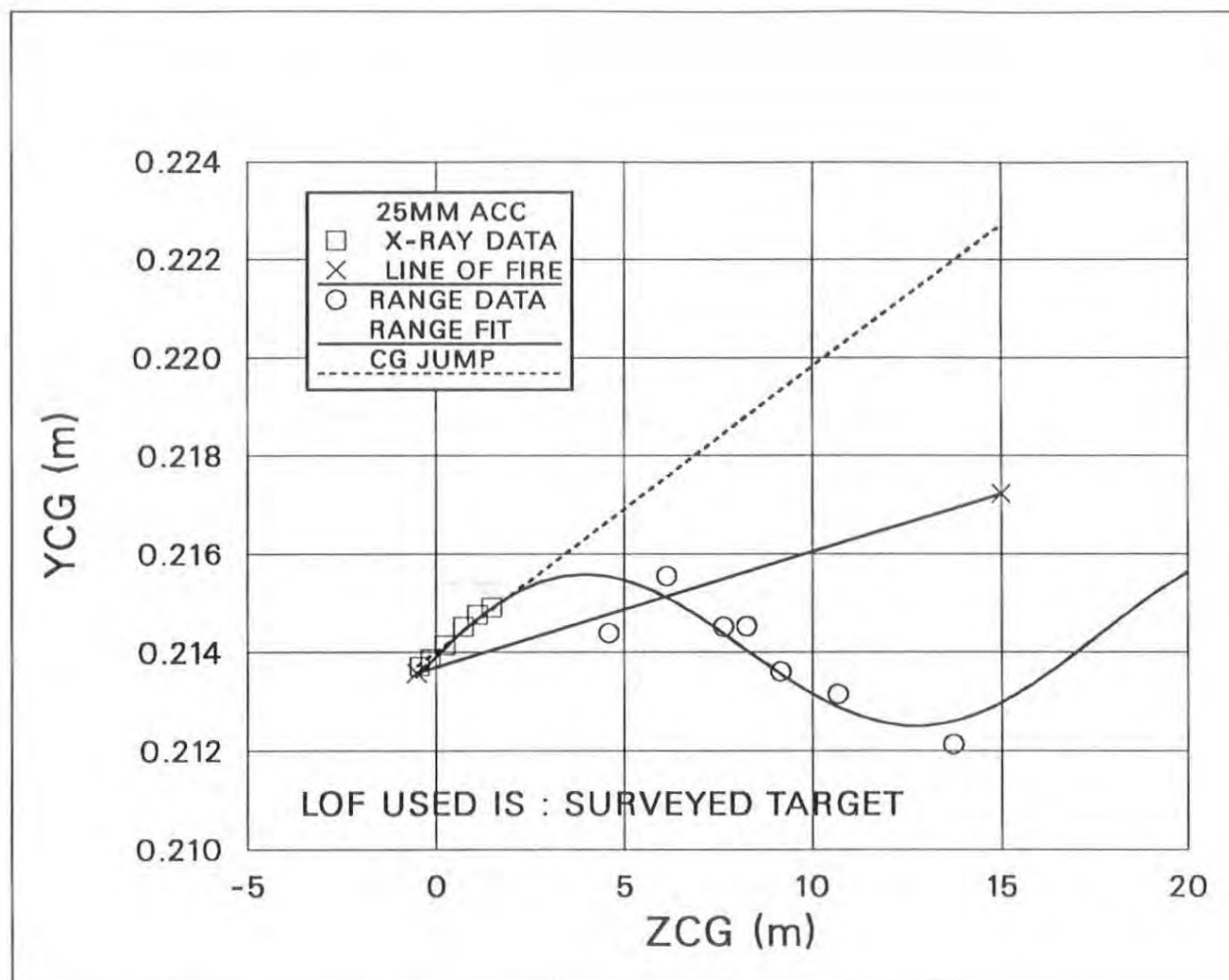


Figure (7) Vertical CG Trajectory of the Projectile

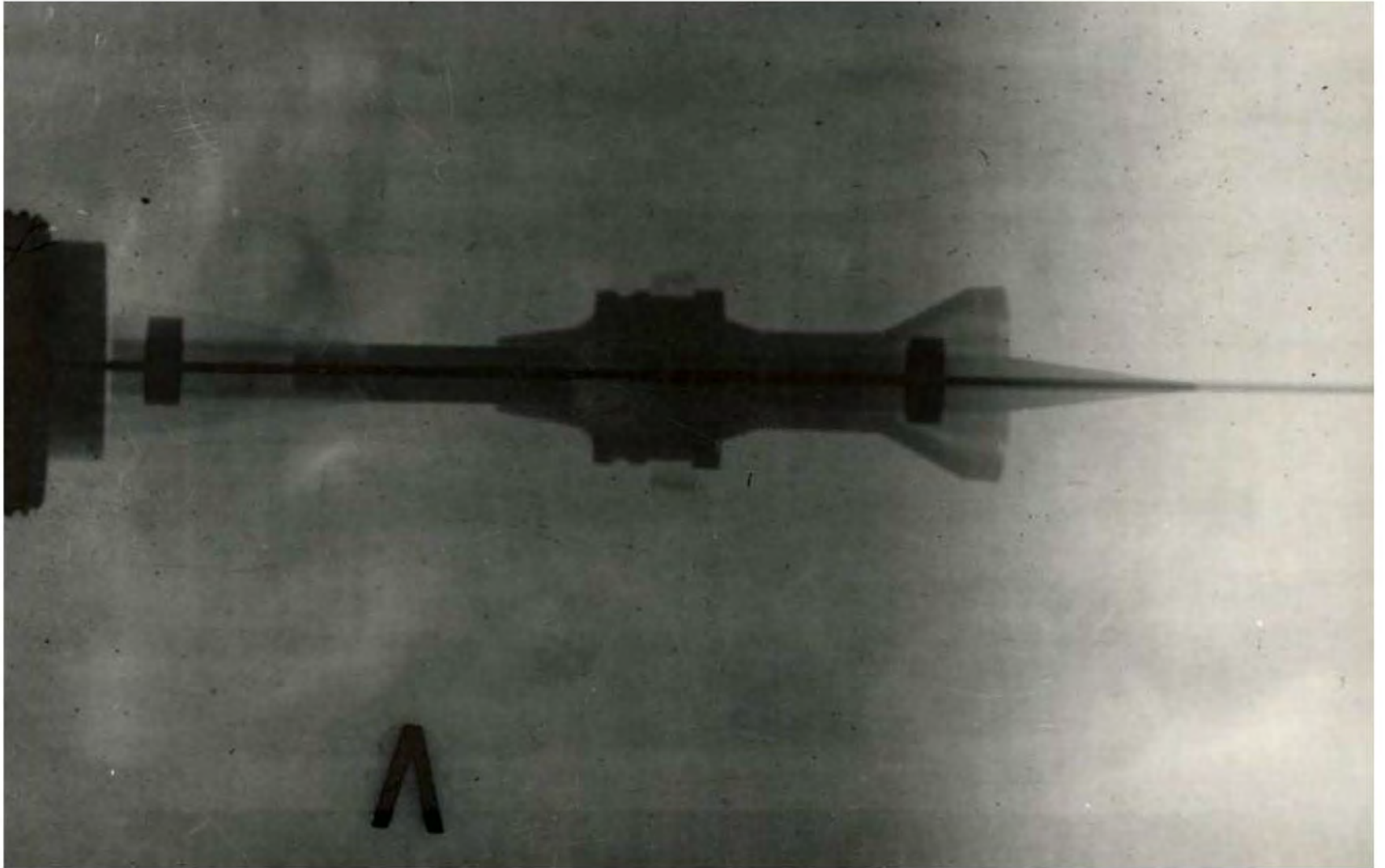


Figure (8a) Vertical X-Ray Image of the Long Wheelbase Design: X-Ray Station #1

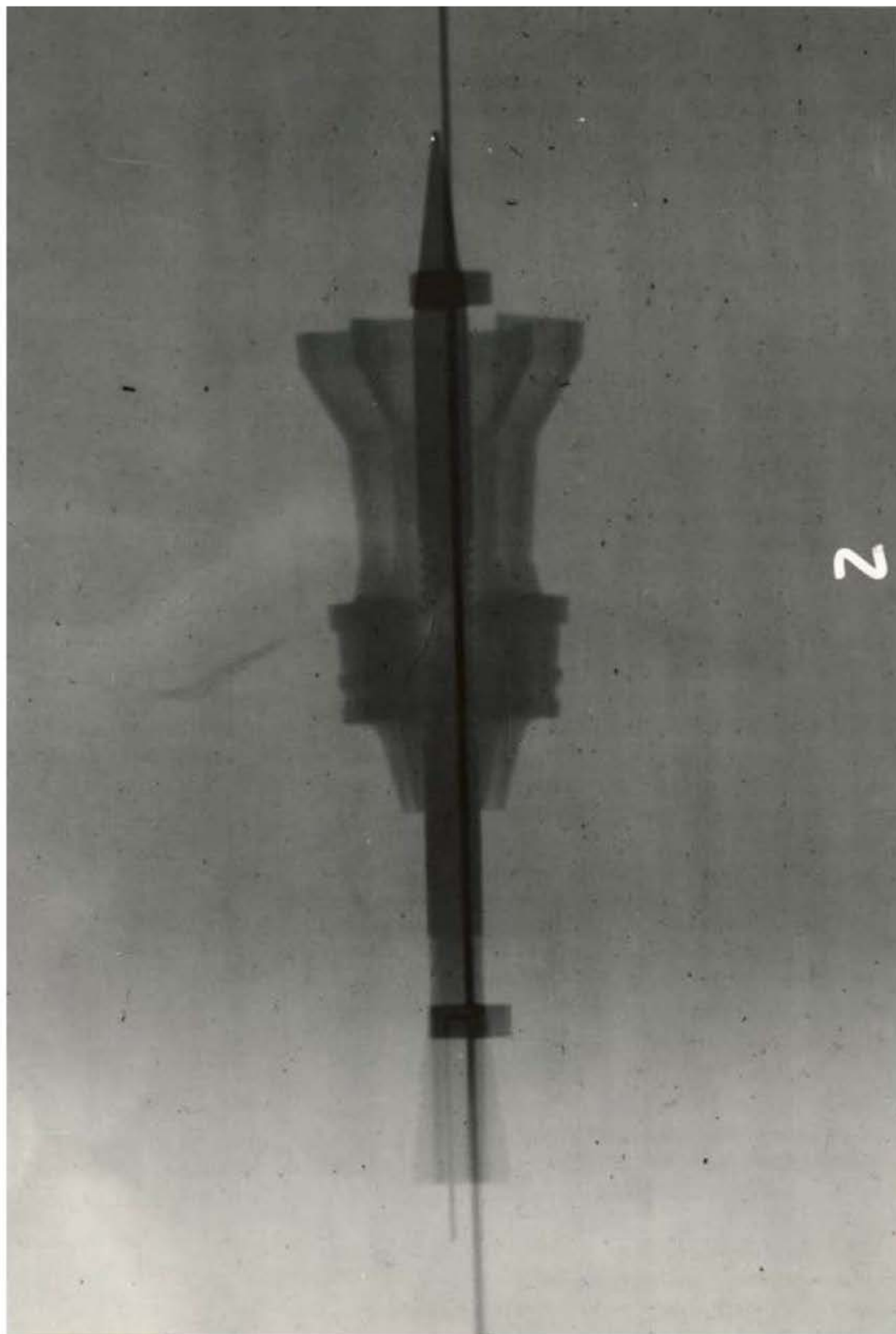


Figure (8b) Vertical X-Ray Image of the Long Wheelbase Design: X-Ray Station #2



Figure (8c) Vertical X-Ray Image of the Long Wheelbase Design: X-Ray Station #3

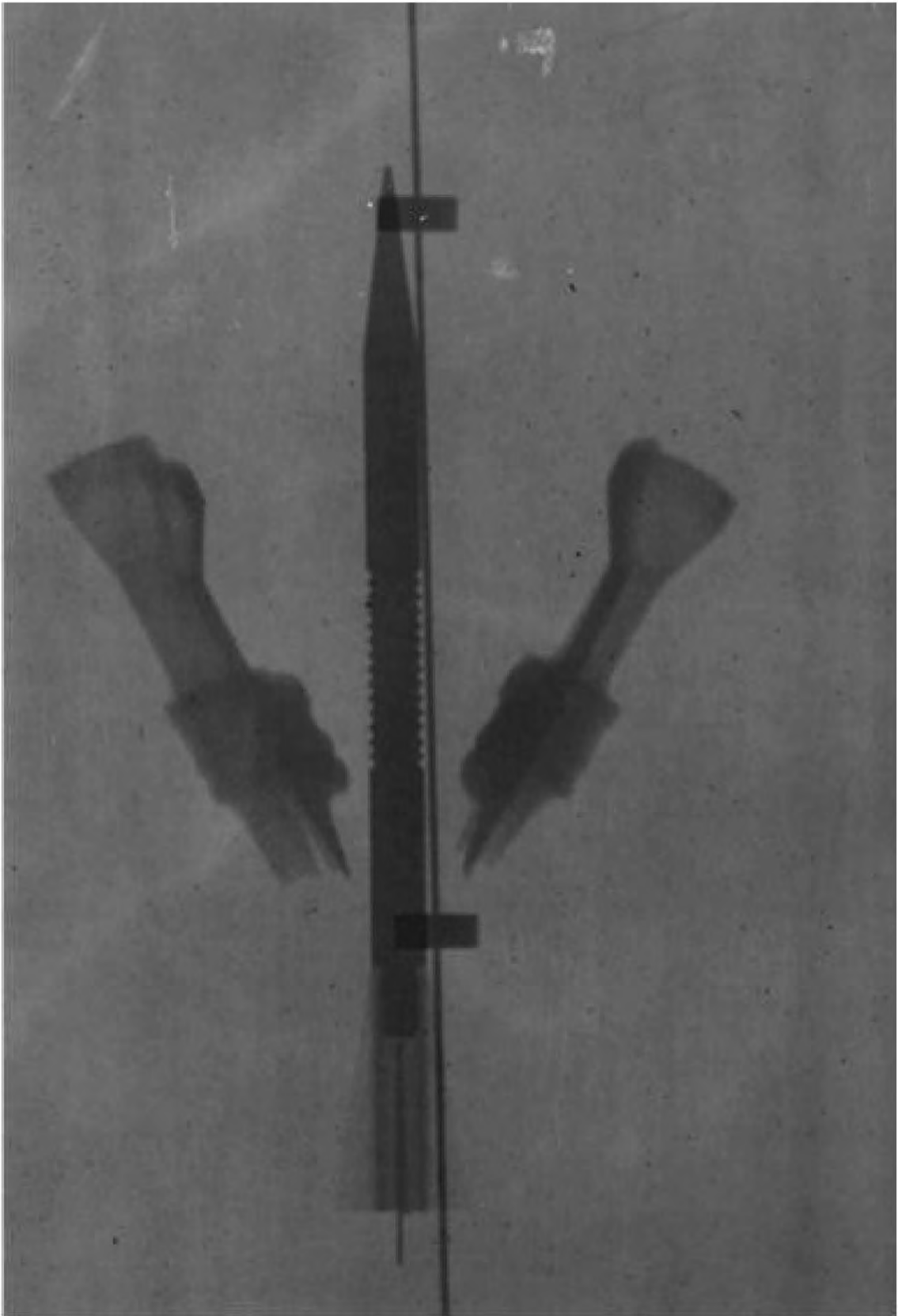


Figure (8d) Vertical X-Ray Image of the Long Wheelbase Design: X-Ray Station #4

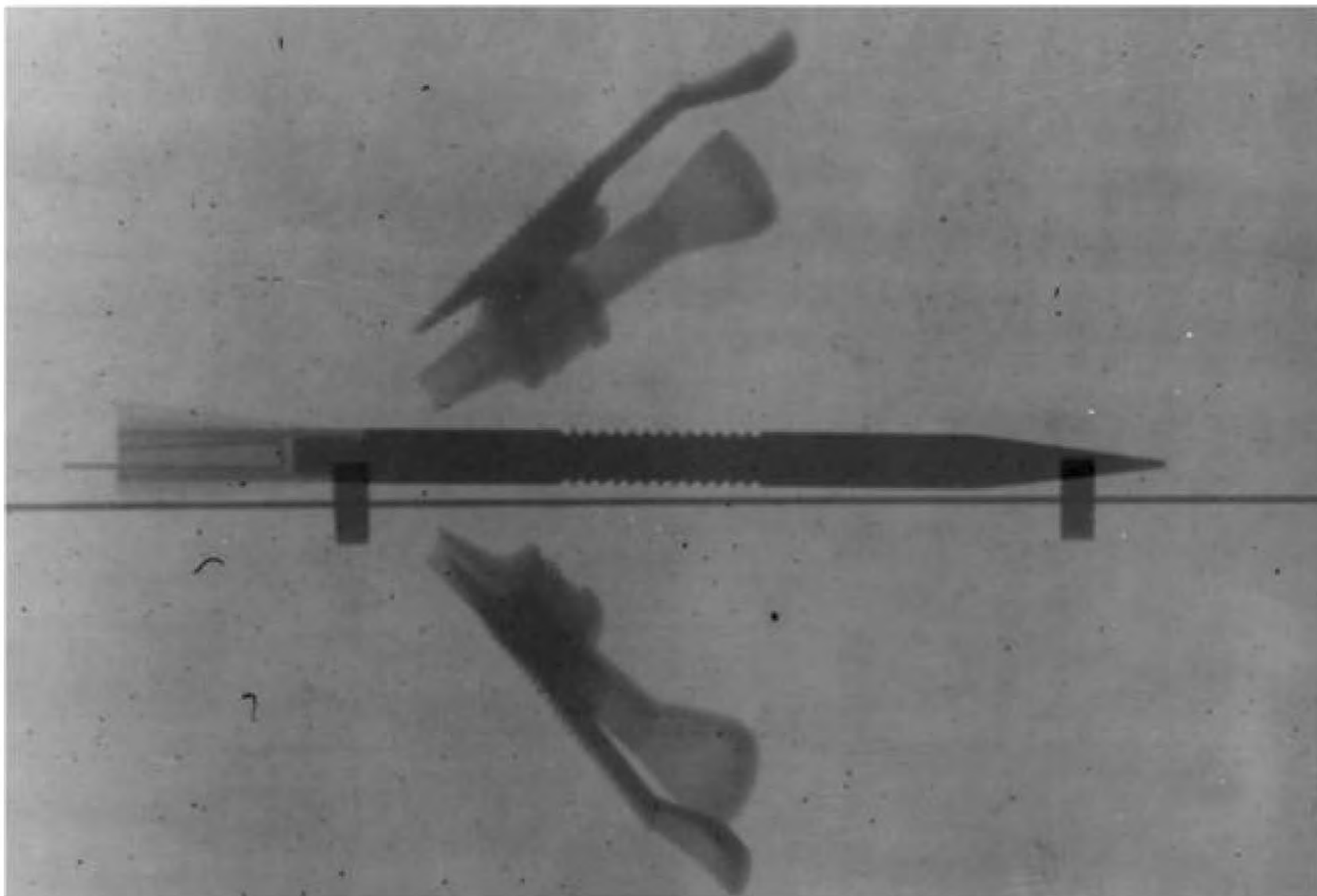


Figure (8e) Vertical X-Ray Image of the Long Wheelbase Design: X-Ray Station #5

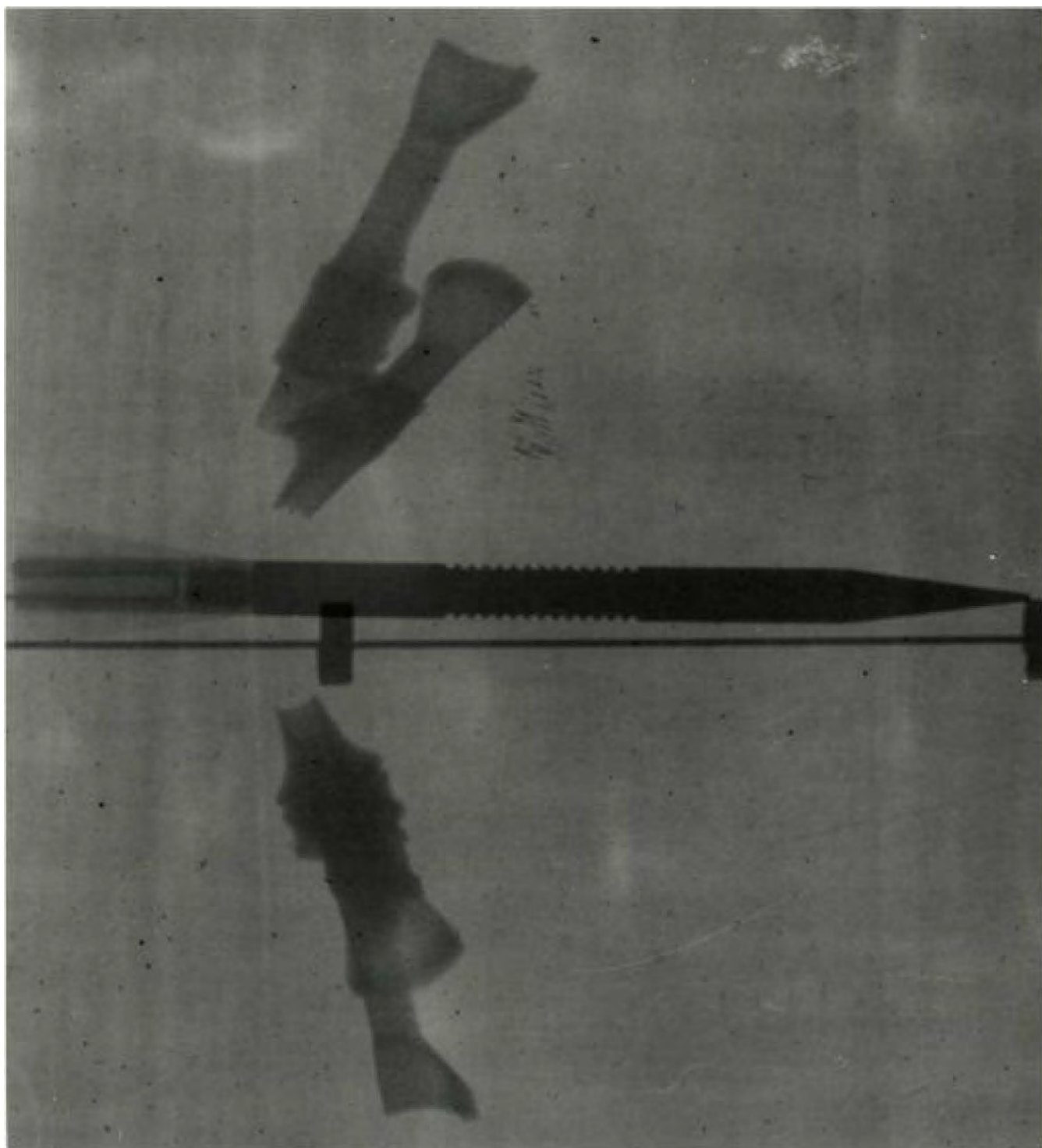


Figure (8f) Vertical X-Ray Image of the Long Wheelbase Design: X-Ray Station #6

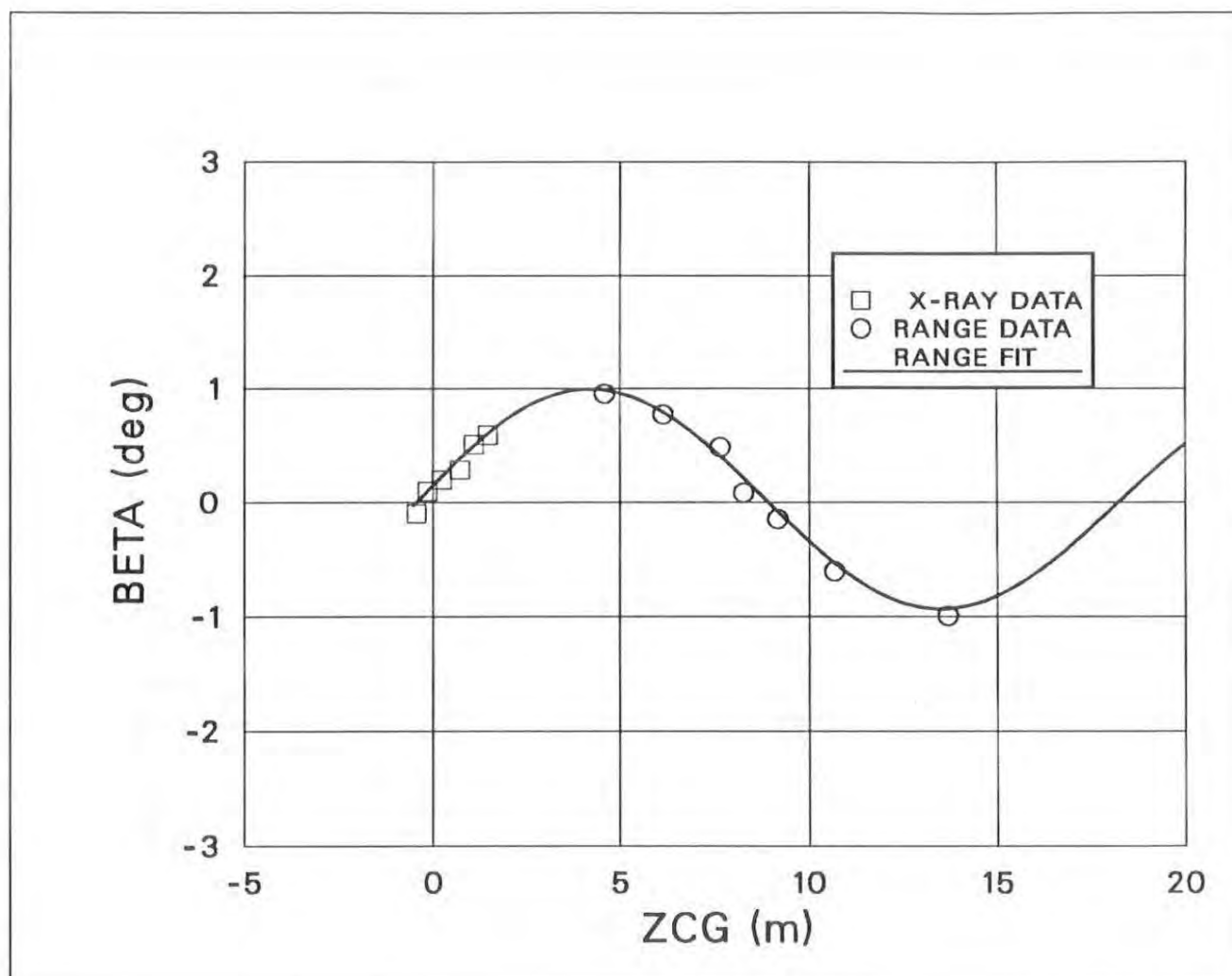


Figure (9) Horizontal Yawing Motion

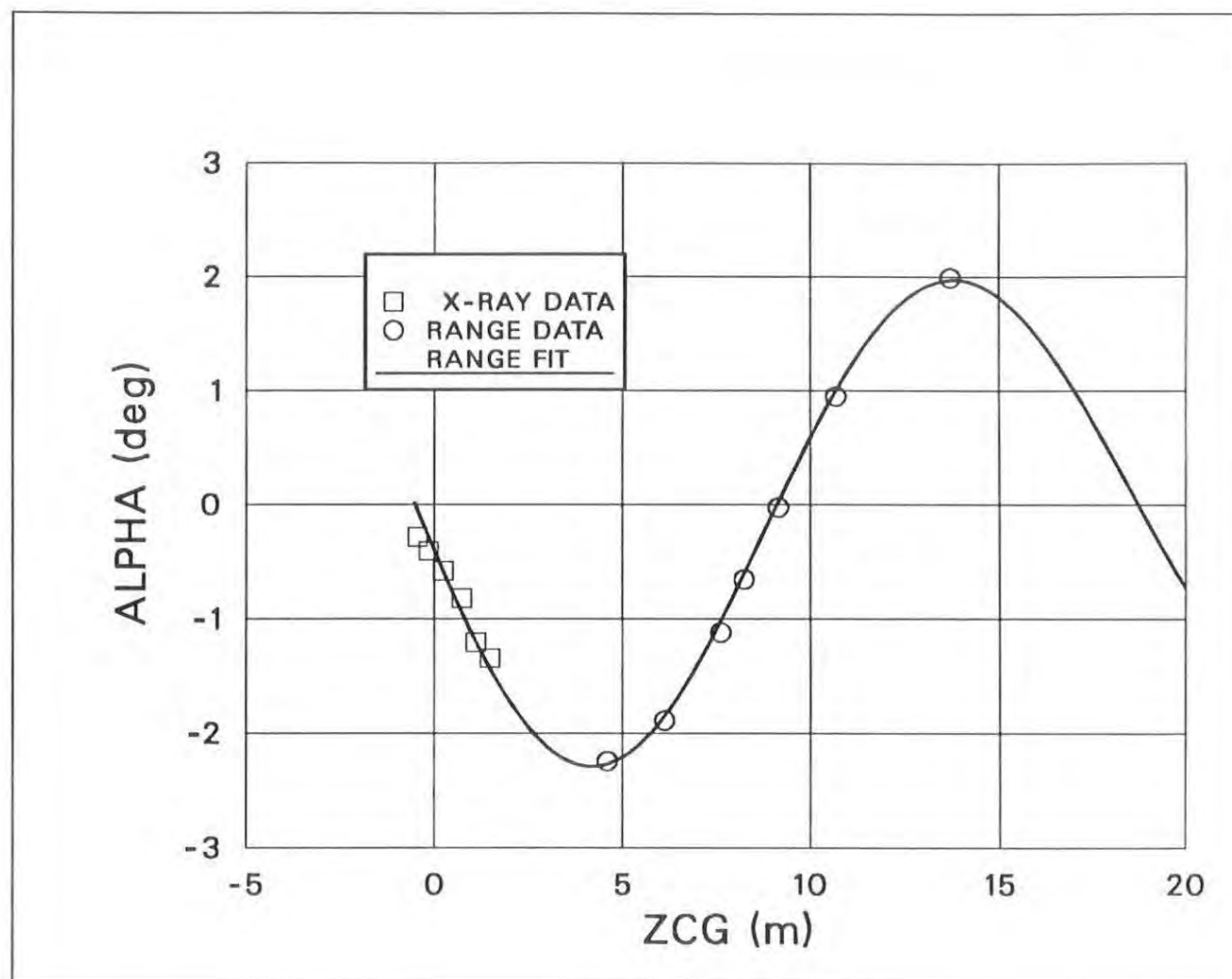


Figure (10) Vertical Yawing Motion

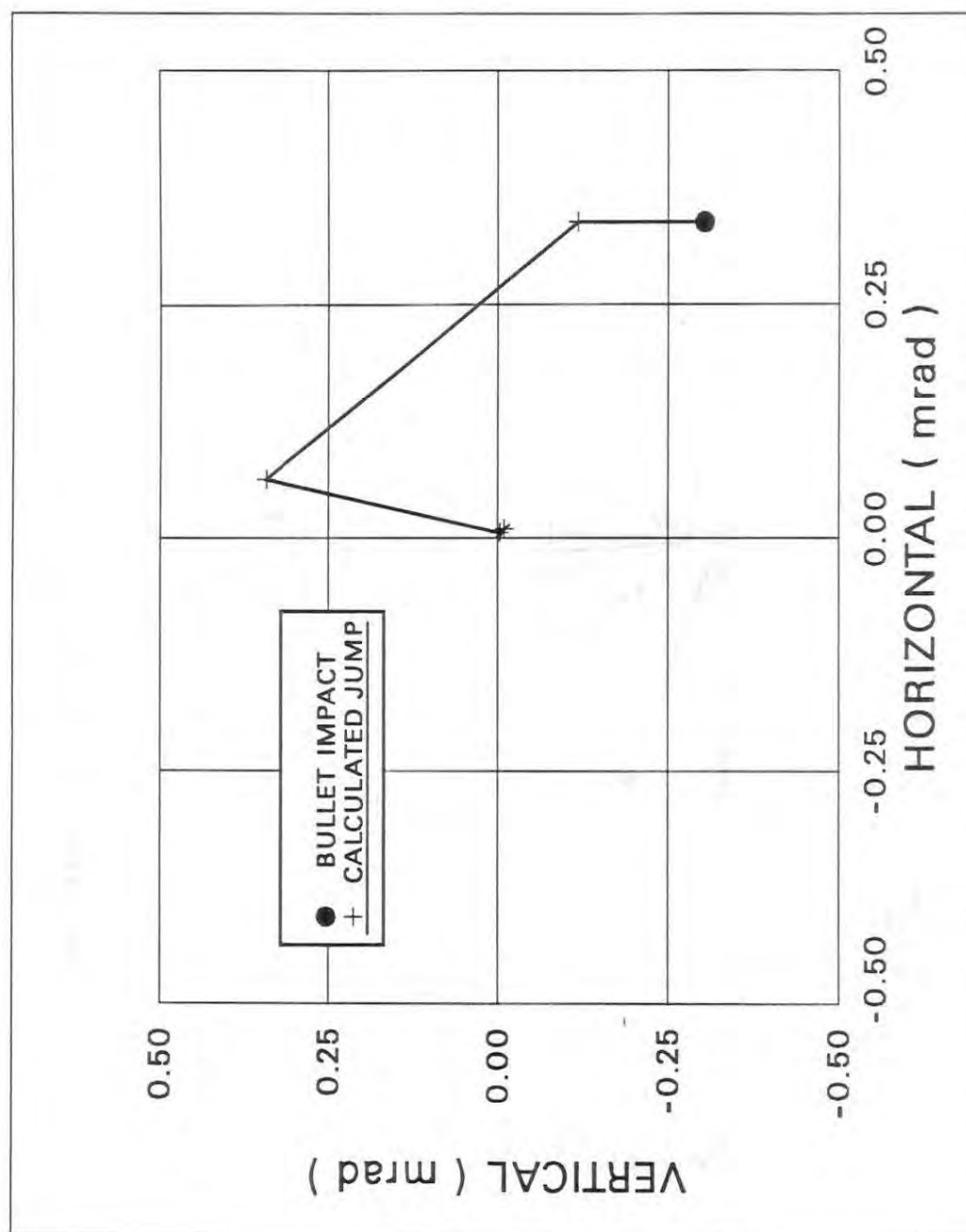


Figure (11) Jump Closure

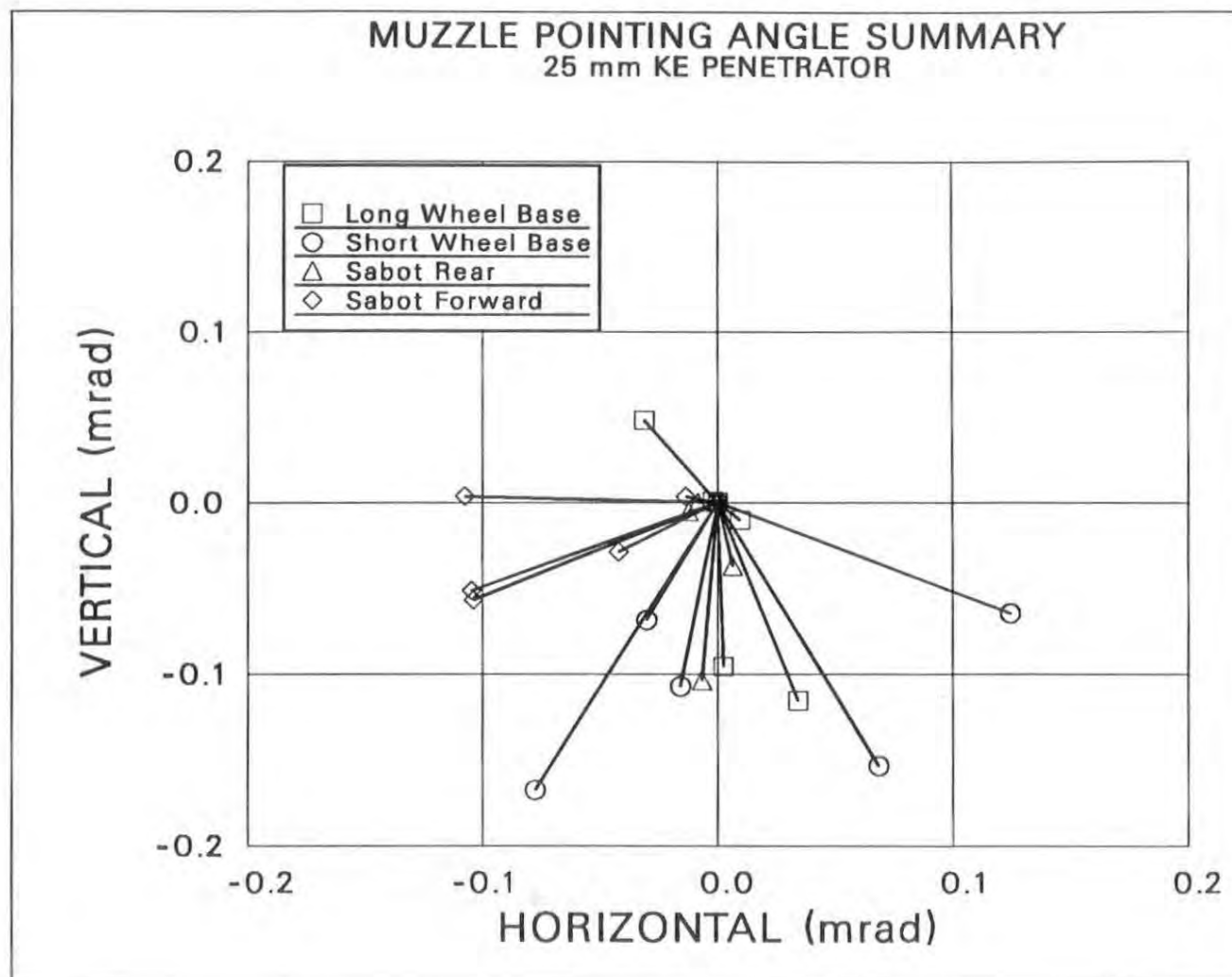


Figure (12) Muzzle Pointing Angle Summary

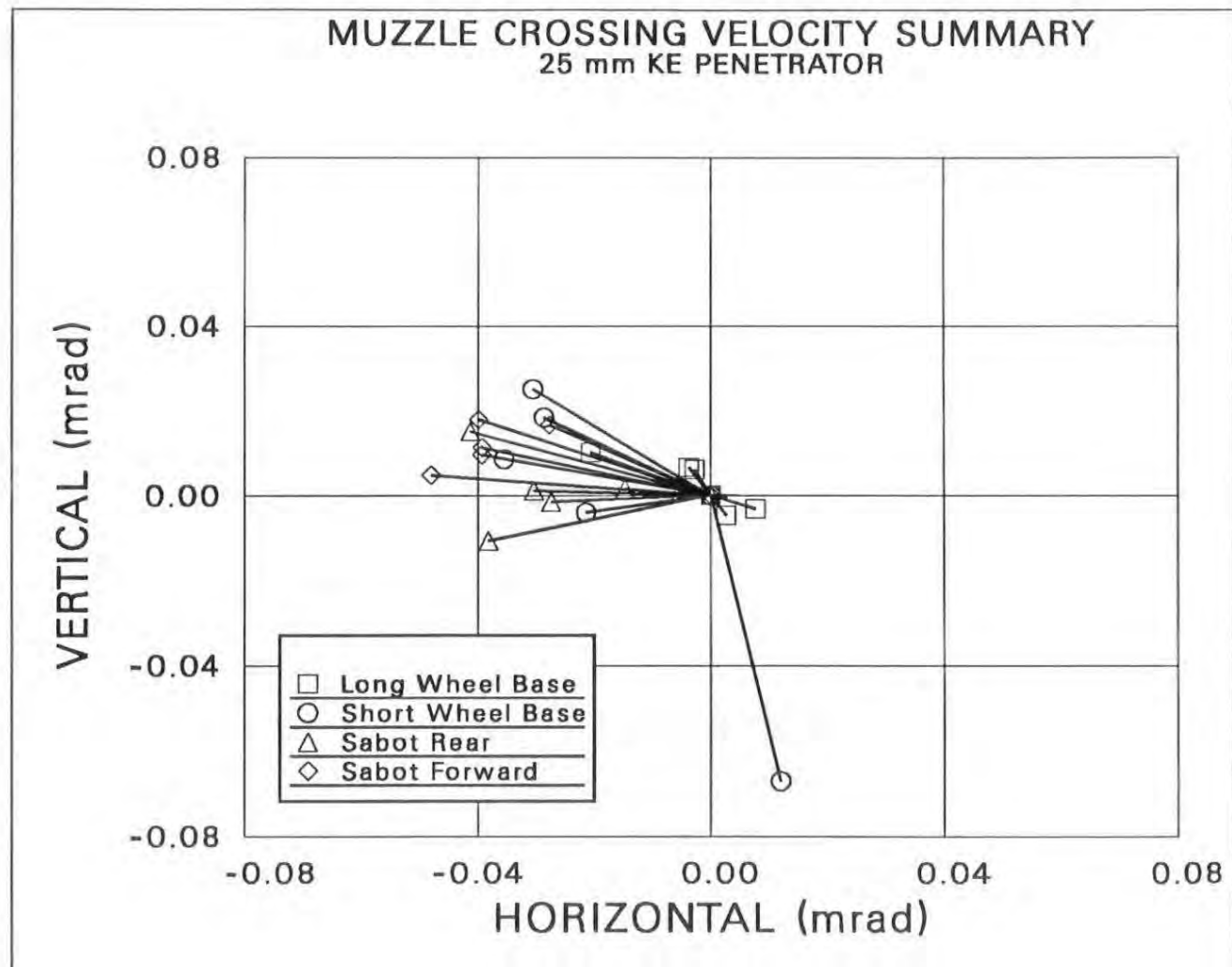


Figure (13) Muzzle Crossing Velocity Summary

Figure (14) Projectile Center of Gravlty Jump Summary

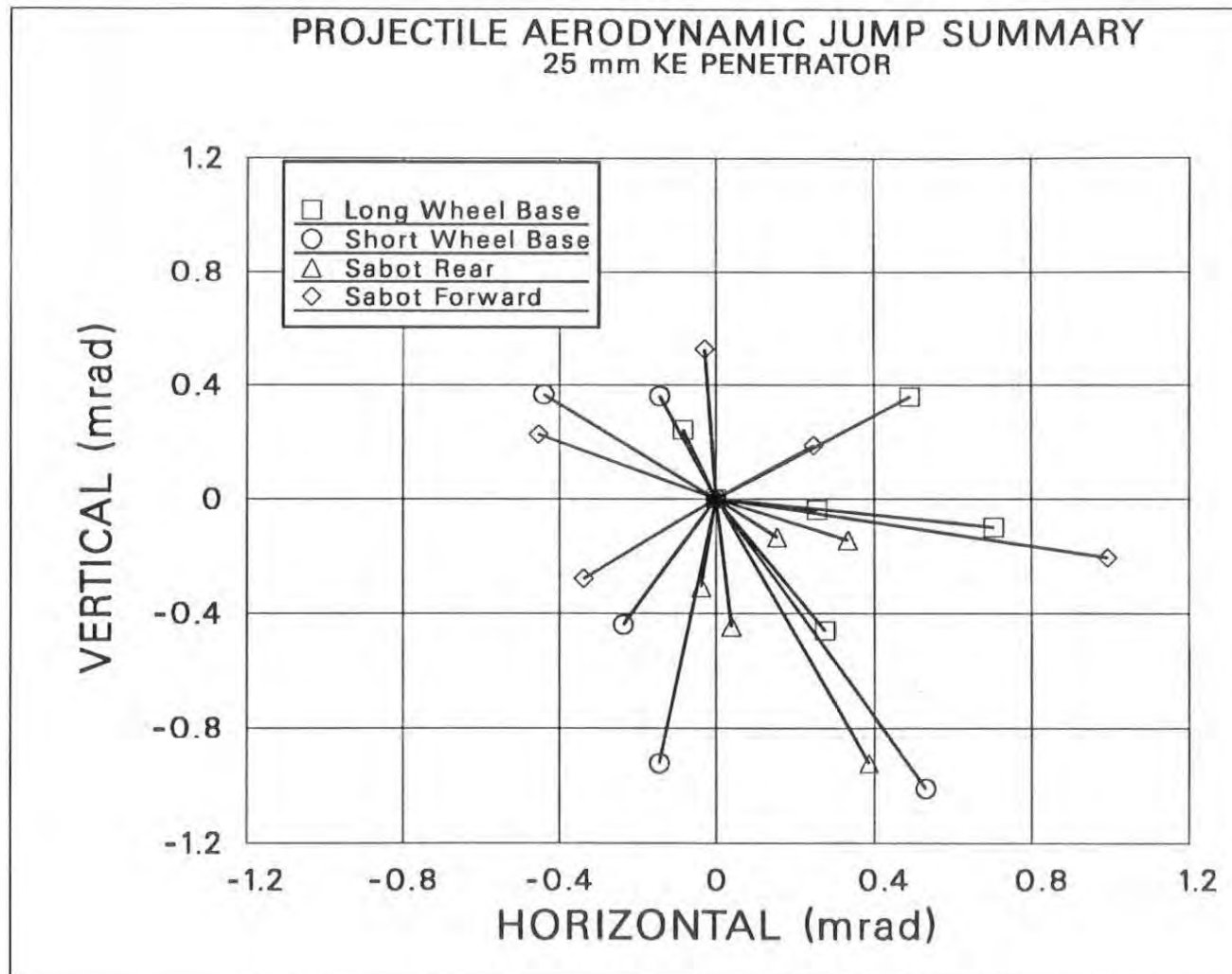


Figure (15) Projectile Aerodynamic Jump Summary

Table (1) Target Mean Impact and Dispersion Summary

Configuration	X_{mean} (mrad)	Y_{mean} (mrad)	σ_x (mrad)	σ_y (mrad)
Long wheelbase	0.24	0.18	0.31	0.29
Short wheelbase	-0.04	-0.26	0.63	0.70
Sabot rear	0.17	-0.37	0.62	0.47
Sabot forward	-0.17	0.02	0.57	0.23

Table (2) Mean Impact and Dispersion Summary: Long Wheelbase Configuration

Component	X_{mean} (mrad)	Y_{mean} (mrad)	σ_x (mrad)	σ_y (mrad)	σ_x^2 (mrad²)	σ_y^2 (mrad²)
Muzzle Pointing Angle (PA)	0.00	-0.03	0.02	0.07	0.0005	0.0047
Muzzle Crossing Velocity (CV)	-0.00	0.00	0.01	0.01	0.0001	0.00004
Projectile CG Jump (CG)	-0.03	0.43	0.12	0.10	0.0132	0.0109
Aerodynamic Jump (AJ)	0.33	-0.00	0.30	0.32	0.0870	0.1027
Cross Correlation ($2\sigma_{\text{CGAJ}}$)	—	—	—	—	0.0296*	0.0170*
Gravity Drop	—	-0.189	—	—	—	—
Sum (Equation 2)	0.30	0.21	0.36	0.37	0.1304	0.1453
Measured Impact	0.24	0.18	0.31	0.29	0.0961	0.0841

* not statistically significant

Table (3) Mean Impact and Dispersion Summary: Short Wheelbase Configuration

Component	X_{mean} (mrad)	Y_{mean} (mrad)	σ_x (mrad)	σ_y (mrad)	σ_x^2 (mrad ²)	σ_y^2 (mrad ²)
Muzzle Pointing Angle (PA)	0.01	-0.11	0.08	0.05	0.0064	0.0025
Muzzle Crossing Velocity (CV)	-0.02	0.00	0.02	0.04	0.0004	0.0016
Projectile CG Jump (CG)	0.05	0.35	0.36	0.32	0.1296	0.1024
Aerodynamic Jump (AJ)	-0.09	-0.33	0.37	0.67	0.1369	0.4489
Cross Correlation ($2\sigma_{\text{CGAJ}}$)	—	—	—	—	0.1344*	-0.0302*
Gravity Drop	—	-0.185	—	—	—	—
Sum (Equation 2)	-0.05	-0.28	0.64	0.72	0.4077	0.5252
Measured Impact	-0.04	-0.26	0.63	0.70	0.3969	0.4900

* not statistically significant

Table (4) Mean Impact and Dispersion Summary: Sabot-Rear Configuration

Component	X_{mean} (mrad)	Y_{mean} (mrad)	σ_x (mrad)	σ_y (mrad)	σ_x^2 (mrad²)	σ_y^2 (mrad²)
Muzzle Pointing Angle (PA)	-0.01	-0.04	0.01	0.04	0.0001	0.0016
Muzzle Crossing Velocity (CV)	-0.03	0.00	0.01	0.01	0.0001	0.0001
Projectile CG Jump (CG)	0.04	0.22	0.56	0.38	0.3136	0.1444
Aerodynamic Jump (AJ)	0.17	-0.39	0.18	0.32	0.0324	0.1024
Cross Correlation ($2\sigma_{\text{CGAJ}}$)	—	—	—	—	0.0912*	0.0112*
Gravity Drop	—	-0.186	—	—	—	—
Sum (Equation 2)	0.17	-0.40	0.66	0.51	0.4374	0.2597
Measured Impact	0.17	-0.37	0.62	0.47	0.3844	0.2209

* not statistically significant

Table (5) Mean Impact and Dispersion Summary: Sabot-Forward Configuration

Component	X_{mean} (mrad)	Y_{mean} (mrad)	σ_x (mrad)	σ_y (mrad)	σ_x^2 (mrad²)	σ_y^2 (mrad²)
Muzzle Pointing Angle (PA)	-0.07	-0.03	0.04	0.03	0.0016	0.0009
Muzzle Crossing Velocity (CV)	-0.04	0.01	0.01	0.01	0.0001	0.0001
Projectile CG Jump (CG)	-0.08	0.14	0.15	0.10	0.0225	0.0100
Aerodynamic Jump (AJ)	0.08	0.09	0.58	0.33	0.3364	0.1089
Cross Correlation ($2\sigma_{\text{CGAJ}}$)	—	—	—	—	0.0248*	-0.0520
Gravity Drop	—	-0.186	—	—	—	—
Sum (Equation 2)	-0.11	-0.02	0.62	0.26	0.3854	0.0679
Measured Impact	-0.17	0.02	0.57	0.23	0.3249	0.0529

* not statistically significant

VI. REFERENCES

- 1.) Plostins, P., Celmins, I. and Bornstein, J.A., "The Effect of Front Sabot Borerider Stiffness on the Launch Dynamics of Fin-Stabilized Kinetic Energy Ammunition," BRL-TR-3047, U.S. Army Ballistic Research Laboratory, Aberdeen Proving Ground, MD 21005, October 1989. (AD A213327)
- 2.) Bornstein, J.A. and Haug, B.T., "Gun Dynamics Measurements for Tank Gun Systems," BRL-MR-3688, U.S. Army Ballistic Research Laboratory, Aberdeen Proving Ground, MD 21005, July 1988. (AD B122913)
- 3.) Schmidt, E.M., Plostins, P., and Bundy, M.L., "Flash Radiographic Diagnostics of Projectile Launch," Proceedings of the 1984 Flash Radiographic Symposium, E.A. Webster, Jr. and A.M. Kennedy, editors, The American Society for Nondestructive Testing, 4135 Arlington Plaza, Columbus, OH 43221, 1984.
- 4.) Bornstein, J.A., Celmins, I., Plostins, P. and Schmidt, E.M., "Launch Dynamics of Fin-Stabilized Projectiles," BRL-MR-3715, U.S. Army Ballistic Research Laboratory, Aberdeen Proving Ground, MD 21005, December 1988. (AD A210713)
- 5.) Braun, W.F., "The Free Flight Aerodynamics Range," BRL-R-1048, U.S. Army Ballistic Research Laboratory, Aberdeen Proving Ground, MD 21005, July 1958. (AD 202249)
- 6.) Murphy, C.H., "Free Flight Motion of Symmetric Missiles," BRL-TR-1216, U.S. Army Ballistic Research Laboratory, Aberdeen Proving Ground, MD 21005, July 1963. (AD 442757)
- 7.) Ott, L., "An Introduction to Statistical Methods and Data Analysis," Duxbury Press, Boston, MA 02116, 1984.

INTENTIONALLY LEFT BLANK.

No of
Copies Organization

- 2 Administrator
Defense Technical Info Center
ATTN: DTIC-DDA
Cameron Station
Alexandria, VA 22304-6145
- 1 HQDA (SARD-TR)
WASH DC 20310-0001
- 1 Commander
U.S. Army Materiel Command
ATTN: AMCDRA-ST
5001 Eisenhower Avenue
Alexandria, VA 22333-0001
- 1 Commander
U.S. Army Laboratory Command
ATTN: AMSLC-DL
2800 Powder Mill Road
Adelphi, MD 20783-1145
- 2 Commander
U.S. Army Armament Research,
Development, and Engineering Center
ATTN: SMCAR-IMI-I
Picatinny Arsenal, NJ 07806-5000
- 2 Commander
U.S. Army Armament Research,
Development, and Engineering Center
ATTN: SMCAR-TDC
Picatinny Arsenal, NJ 07806-5000
- 1 Director
Benet Weapons Laboratory
U.S. Army Armament Research,
Development, and Engineering Center
ATTN: SMCAR-CCB-TL
Watervliet, NY 12189-4050
- 1 Commander
U.S. Army Armament, Munitions
and Chemical Command
ATTN: SMCAR-ESP-L
Rock Island, IL 61299-5000
- 1 Director
U.S. Army Aviation Research
and Technology Activity
ATTN: SAVRT-R (Library)
M/S 219-3
Ames Research Center
Moffett Field, CA 94035-1000

No of
Copies Organization

- 1 Commander
U.S. Army Missile Command
ATTN: AMSMI-RD-CS-R (DOC)
Redstone Arsenal, AL 35898-5010
- 1 Commander
U.S. Army Tank-Automotive Command
ATTN: ASQNC-TAC-DIT (Technical
Information Center)
Warren, MI 48397-5000
- 1 Director
U.S. Army TRADOC Analysis Command
ATTN: ATRC-WSR
White Sands Missile Range, NM 88002-5502
- (Class. only)1 Commandant
U.S. Army Infantry School
ATTN: ATSH-CD (Security Mgr.)
Fort Benning, GA 31905-5660
- (Unclass. only)1 Commandant
U.S. Army Infantry School
ATTN: ATSH-CD-CSO-OR
Fort Benning, GA 31905-5660
- 1 Air Force Armament Laboratory
ATTN: AFATL/DLODL
Eglin AFB, FL 32542-5000

Aberdeen Proving Ground
- 2 Dir, USAMSAA
ATTN: AMXSY-D
AMXSY-MP, H. Cohen
- 1 Cdr, USATECOM
ATTN: AMSTE-TD
- 3 Cdr, CRDEC, AMCCOM
ATTN: SMCCR-RSP-A
SMCCR-MU
SMCCR-MSI
- 1 Dir, VLAMO
ATTN: AMSLC-VL-D
- 10 Dir, BRL
ATTN: SLCBR-DD-T

<u>No. of</u> <u>Copies</u>	<u>Organization</u>
5	<p>Commander U.S. Army Armament Research, Development, and Engineering Center ATTN: SMCAR-CCL-CA, P. O'Neill C. A. Miller E. Malatesta G. Fleming Alan Li Picatinny Arsenal, NJ 07806-5000</p>
4	<p>Commander U.S. Army Armament Research, Development, and Engineering Center ATTN: SMCAR-AEI-A, R. Kline J. Grau Chiu Ng J. Whyte Picatinny Arsenal, NJ 07806-5000</p>
1	<p>Commander U.S. Army Armament Research, Development, and Engineering Center ATTN: AMSMC-QAF-S, D. Messer Picatinny Arsenal, NJ 07806-5000</p>
3	<p>Commandant U.S. Army Infantry School ATTN: ATSH-CD-MLS-S, SFC Kohlase ATSH-INA-BPO, SFC Wood ATSH-TD-S-D, V. Hartman Fort Benning, GA 31905-5800</p>
1	<p>Director HQ, TRAC RPD ATTN: ATCD-MH, CPT J. Williams Fort Monroe, VA 23651-5000</p>
1	<p>Commander U.S. Army Yuma Proving Ground ATTN: STEYP-MT-ET-C, W. Aynes Yuma, AZ 85365-9103</p>

<u>No. of</u> <u>Copies</u>	<u>Organization</u>
1	<p>Commander U.S. Army Tank-Automotive Command Program Manager Bradley Fighting Vehicle System ATTN: AMCPM-BFVS, K. Pitco Warren, MI 48937-5000</p>
1	<p>Commander U.S. Army Armor Center and School ATTN: ATSB-SMT, MAJ Newlin Fort Knox, KY 40121</p>
2	<p>Alliant Techsystems, Inc. ATTN: C. Rippe B. Becker 600 Second Street, N.E. Hopkins, MN 55343</p>
3	<p>Aerojet General Corporation ATTN: E. Daniels J. Parkinson S. Rush P.O. Box 296 Azusa, CA 91702</p>
2	<p>Arrow Tech Associates, Inc. ATTN: B. Whyte W. Hathaway P.O. Box 4218 South Burlington, VT 05401-0042</p>
	<p><u>Aberdeen Proving Ground</u></p>
4	<p>Dir, USACSTA ATTN: STECS-AA-LA, M. Maule J. Steier M. Feinberg A. Rose</p>
1	<p>Dir, USATECOM ATTN: AMSTE-TER, B. Marshall</p>
2	<p>Dir, USAMSAA ATTN: AMXSU-GI, D. Hartka CPT Klimack</p>